Insight into Elastic Properties of Binary Alkali Silicate Glasses; Prediction and Interpretation through Atomistic Simulation Techniques

Alfonso Pedone,[†] Gianluca Malavasi,[†] Alastair N. Cormack,[‡] Ulderico Segre,[†] and M. Cristina Menziani*[,†]

Dipartimento di Chimica, Università di Modena e Reggio Emilia, Via G. Campi 183, 41100 Modena, Italy, and Kazuo Inamori School of Engineering, New York State College of Ceramics, Alfred University, Alfred, New York 14802

Received November 2, 2006. Revised Manuscript Received March 30, 2007

Molecular dynamics simulations and energy-minimization techniques have been applied for the first time to determine the whole set of elastic properties (Young's modulus, shear modulus, bulk modulus, and Poisson's ratio) of alkali silicate glasses with different ion modifiers (Li, Na, and K) in the range 0−30 mol % alkaline oxide. Excellent agreement has been found between the simulation results and the experimental data. The peculiar behavior of the Li-containing glasses with respect to the Na and K ones is extensively discussed in terms of the glass structural features. It is found that the elastic property variation as a function of alkali addition can be explained by three concurrent factors: (1) depolymerization of the silica network; (2) increasing the cohesion of the glass by the establishment of alkali−NBO bonds; and (3) decreasing the free volume with consequent increasing of the glass packing density.

1. Introduction

Multicomponent silicate glasses are of great importance in both the fields of technological industries and geosciences. They find wide applications as substrates for electronic displays, optical fibers, thick-film packaging, optical disc, aerospace and high-performance composites, medical and dental implants, and radiation shielding. From a practical point of view, the mechanical properties of a glass often dictate whether a specific need or application can be met. Therefore, the prediction of these properties according to glass composition is becoming increasingly indispensable for developing materials with a greater focus on end-user application requirements, reduction of development costs, and a decrease in the time to market.

However, theoretical or numerical studies of the mechanical properties of glasses have been scarce.

Most of the studies in the field rely basically on statistical processing of available experimental information collected in glass databases.[1] In spite of quite significant differences between the empirical methods used they share two important drawbacks: (a) the presence or absence of the experimental data required to determine the parameters limits the possibility of extending the calculation to a wide range of compositions; (b) their objective is exclusively predictive, and no rigorous quantitative explanation for the observed property−composition dependence is offered.

Nowadays, atomistic simulation techniques as molecular dynamics (MD) simulations and energy minimization are becoming very valuable alternatives because they allow the study and understanding of material properties in direct connection to the microscopic structure. Although these techniques are well-established in the literature, to the best of our knowledge, no computational investigations on composition dependence of mechanical properties of multicomponent glasses have been performed so far.

In fact, most of the studies focused on MD simulations of v-SiO_2. Huang et al.[2] studied the thermomechanical properties and polymorphisms of v-SiO_2, whereas Muralidharan et al.[3] employed MD simulations to study brittle fracture. Moreover, the first attempts to estimate the mechanical properties of Na_2O-SiO_2 and SiO_2 glasses overestimated the Young's modulus by 1 order of magnitude.[4,5]

This work represents the first detailed systematic computational study of the mechanical properties (Young's modulus, shear modulus, bulk modulus, and Poisson's ratio) of wide series of alkali silicate glasses obtained by means of the MD and energy-minimization methods.

The consequences of the addition of alkali oxides to silica glass have been the object of many studies for a long time. The structure of alkali silicate glasses has been well-characterized by NMR,[6−12] IR[13] and Raman[14] spectroscopy,

* Corresponding author. E-mail: menziani@unimo.it. Tel.: 39 059 2055091. Fax: 39 059 373543.
[†] Università di Modena e Reggio Emilia.
[‡] Alfred University.

(1) Priven, A. I. *Glass Technol.* **2004**, *45*, 244.
(2) Huang, L.; Duffrène, L.; Kieffer, J. *J. Non-Cryst. Solids* **2004**, *349*, 1−9.
(3) Muralidharan, K.; Simmons, J. H.; Deymier, P. A.; Runge, K. *J. Non-Cryst. Solids* **2005**, *351*, 1532−1542.
(4) Soules, T. F. *J. Non-Cryst. Solids* **1982**, *49*, 29.
(5) Soules, T. F.; Busbey, R. F. *J. Chem. Phys.* **1983**, *78*, 6307.
(6) Maekawa, H.; Maekawa, T.; Kawamura, K.; Yokokawa, T. *J. Non-Cryst. Solids* **1991**, *127*, 53.
(7) Voigt, U.; Lammert, H.; Eckert, H.; Heuer, A. *Phys. Rev. B* **2005**, *72*, 64207.
(8) Dupree, R.; Holland, D.; Williams, D. S. *J. Non-Cryst. Solids* **1986**, *81*, 185.

10.1021/cm062619r CCC: $37.00
Published on Web 05/25/2007

Table 1. Molar Composition, Number of Atoms, Densities, and Cell Sizes of the $xM_2O-(100-x)SiO_2$ Simulated Glasses (M = Li, Na, K); Total Number of Atoms in Each Box is 1536

		no. of atoms in the simulation box				
formulation	xM_2O (mol %)	Li/Na/K	Si	O	density (g/cm^3)	cell size (Å)
SiO_2	0	0	512	1024	2.200	28.5290
LS10	10	102	461	973	2.246	27.8519
LS15	15	154	435	947	2.269	27.5066
LS20	20	204	410	922	2.292	27.1694
LS25	25	256	384	896	2.314	26.8245
LS30	30	308	358	870	2.334	26.4848
NS10	10	102	461	973	2.294	28.1633
NS15	15	154	435	947	2.340	27.9924
NS20	20	204	410	922	2.385	27.8294
NS25	25	256	384	896	2.428	27.6788
NS30	30	308	358	870	2.469	27.5393
KS10	10	102	461	973	2.305	28.6087
KS15	15	154	435	947	2.347	28.6935
KS20	20	204	410	922	2.390	28.7611
KS25	25	256	384	896	2.429	28.8512
KS30	30	308	358	870	2.466	28.9454

EXAFS,[15,16] and neutron[17−21] and X-ray diffractions, as well as molecular dynamics simulation techniques.[7,22−30]

The structural units of silica glass consist of SiO_4 tetrahedra that share bridging oxygens (BO), establishing a strongly connected three-dimensional network. Disorder in the structure is mainly due to variation in bond and torsion angles.[21] The introduction of alkali ions results in the formation of nonbridging oxygens (NBO) by disruption of the Si−O−Si bonds and consequent reduction in glass connectivity.[31] How these structural modifications are related to the mechanical behavior of alkali silicate glasses is not trivial. In fact, Brillouin scattering measurements have shown an opposite effect on the elastic constants in lithium and potassium silicate glasses,[32,33] and a nonlinear dependence of the elastic constant C_{11} on sodium oxide concentrations has been observed by Vaills et al.[34]

This paper shows that computational simulations can be considered invaluable tools for obtaining both correct numerical estimations of the mechanical properties of interest and atomistic three-dimensional models for the interpretation of the variation of the observed property.

The paper is organized as follows: the computational methods employed for studying the structure, the network dynamics and the elastic properties are discussed in the next section. The results are reported in section 3, together with the discussion of structural and vibrational features responsible for the predicted elastic properties. Finally, in section 4, we offer some conclusions.

2. Computational Methods

2.1. Simulation Procedure. The structures of alkali silicate glasses of composition $xM_2O\cdot(100-x)SiO_2$ (with $x = 0$, 10, 15, 20, 25, and 30 mol % for M = Li, Na, and K) have been modeled by means of NVT Molecular Dynamics (MD) simulations. For each composition, 1536 atoms were placed randomly in a cubic box; three simulations were carried out with different starting configurations. Atomic compositions and size length of the simulation boxes are reported in Table 1, together with the glass densities at room temperature calculated according to Appen's empirical method.[35]

The DL_POLY[36] package has been employed for MD simulations. Integration of the equation of motion has been performed using the Verlet Leapfrog algorithm with a time step of 2 fs. Coulombic interactions have been calculated by the Ewald summation method[37] with a cutoff of 12 Å and an accuracy of 1×10^{-4}. The short range interaction cutoff was set to 5.5 Å.

A pairwise potential recently developed by us has been employed.[38] This is based on a rigid ionic model, with partial charges to handle the partial covalency of silicate systems. The potential is given by the sum of three terms: (i) the long-range Coulombic

(9) Dupree, R.; Holland, D.; Mortuza, M. G. *J. Non-Cryst. Solids* **1990**, *116*, 148.
(10) Sen, S.; Gerardin, C.; Navrotsky, A.; Dickinson, J. E. *J. Non-Cryst. Solids* **1994**, *168*, 64.
(11) Sen, S.; Youngman, R. E. *J. Non-Cryst. Solids* **2003**, *331*, 100.
(12) Eckert, H.; Elbert, S.; Epping, J. D.; Janssen, M.; Kalwei, M.; Strojek, W.; Voigt, U. *Top. Curr. Chem.* **2004**, *246*, 195.
(13) Sitarz, M.; Mozgawa, W.; Handke, M. *J. Mol. Struct.* **1999**, *281*, 511−512.
(14) Lin, C. C.; Huang, L. C.; Shen, P. *J. Non-Cryst. Solids* **2005**, *351*, 3195.
(15) Henderson, G. S. *J. Non-Cryst. Solids* **1995**, *183*, 43.
(16) Mazzara, C.; Jupille, J.; Flank, A. M.; Lagarde, P. *J. Phys. Chem. B* **2000**, *104*, 3438.
(17) Zhao, J.; Gaskell, P. H.; Cluckie, M. M.; Soper, A. K. *J. Non-Cryst. Solids* **1998**, *232*, 721.
(18) Hannon, A. C.; Vessal, B.; Parker, J. M. *J. Non-Cryst. Solids* **1992**, *150*, 97.
(19) Uhlig, H.; Hoffmann, M. J.; Lamparter, H. P.; Aldiger, F.; Bellissent, R.; Steeb, S. *J. Am. Ceram. Soc.* **1996**, *79*, 2833.
(20) Misawa, M.; Price, D. L.; Suzuki, K. *J. Non-Cryst. Solids* **1980**, *37*, 85.
(21) Wright, A. C.; Clare, A. G.; Bachra, B.; Sinclair, R. N.; Hannon, A. C.; Vessal, B. *Trans. Am. Crystallogr. Assoc.* **1991**, *27*, 239.
(22) Smith, W.; Greaves, G. N.; Gillian, M. J. *J. Chem. Phys.* **1995**, *103*, 3091.
(23) Yuan, X.; Cormack, A. N. *J. Non-Cryst. Solids* **2001**, *283*, 69.
(24) Du, J.; Cormack, A. N. *J. Non-Cryst. Solids* **2004**, *349*, 66.
(25) Du, J.; Corrales, R. *Phys. Rev. B* **2005**, *72*, 1.
(26) Du, J.; Corrales, R. *J. Non-Cryst. Solids* **2006**, *352*, 3255.
(27) Jund, P.; Kob, W.; R. J. *Phys. Rev. B* **2001**, *64*, 134303.
(28) Banhatti, D. R.; Heuer, A. *Phys. Chem. Chem. Phys.* **2001**, *3*, 5104−5108.
(29) Heuer, A.; Kunow, M.; Vogel, M.; Banhatti, R. D. *Phys. Chem. Chem. Phys.* **2002**, *4*, 3185−3192.
(30) Lammert, H.; Heuer, A. *Phys. Rev. B* **2005**, *B72*, 214202.
(31) Lammert, H.; Kunow, M.; Heuer, A. *Phys. Rev. Lett.* **2003**, *90*, 215901.
(32) Hushur, A.; Kojima, S.; Kodama, M.; Whittington, B.; Olesiak, M.; Affatigato, M.; Feller, A. *Jpn. J. Appl. Phys.* **2005**, *44*, 6683.
(33) Shaw, R. R.; Uhlmann, D. R. *J. Non-Cryst. Solids* **1971**, *5*, 237.
(34) Vallis, Y.; Luspin, Y.; Hauret, G. *Mater. Sci. Eng., B* **1996**, *40*, 199.
(35) *SciGlass 3.5*; SciVision: Burlington, VT, 1997.
(36) Smith, W.; Forester, T. R. *J. Mol. Graphics* **1996**, *14*, 136.
(37) Ewald, P. P. *Ann. Phys.* **1921**, *64*, 253.
(38) Pedone, A.; Malavasi, G.; Menziani, M. C.; Cormack, A. N.; Segre, U. *J. Phys. Chem. B* **2006**, *110*, 11780−11795.

Table 2. Potential Parameters for Eq 1

	D_{ij} (eV)	a_{ij} (Å^{-1})	r_0 (Å)	C_{ij} (eV Å^{12})
$Li^{0.6}-O^{-1.2}$	0.001080	3.429361	2.680018	1.0
$Na^{0.6}-O^{-1.2}$	0.023363	1.763867	3.006315	5.0
$K^{0.6}-O^{-1.2}$	0.011612	2.062605	3.305308	5.0
$Si^{2.4}-O^{-1.2}$	0.340554	2.006700	2.100000	1.0
$O^{-1.2}-O^{-1.2}$	0.042395	1.379316	3.618701	100.0

potential; (ii) the short-range forces, which are represented by a Morse function; (iii) an additional repulsive term C/r^{12}, which has been added to model the repulsive contribution at high-temperature and pressure. The expression for the model potential is

$$U(r) = \frac{z_i z_j e^2}{r} + D_{ij}[\{1 - \exp[-a_{ij}(r - \bar{r}_{ij})]\}^2 - 1] + \frac{C_{ij}}{r^{12}} \quad (1)$$

where z_i, z_j, D_j, a_{ij}, $\bar{r}_{ij}$, and C_{ij} are parameters and the indices i and j refer to the different atomic species. The atomic charge for an alkali ion is assumed to be $q = +0.6e$, and the values of z_i for the other atoms are taken accordingly. The values of the other parameters in eq 1 are listed in Table 2. They were derived by fitting both structural and mechanical properties of inorganic oxides according to the procedure implemented in the GULP code.[39]

Experience from recent work has led to an optimum glass-forming procedure, where a rigid ionic model with partial charges interatomic potential has been employed.[38,40,41] The systems have been cooled down uniformly from 5000 to 300 K, by decreasing the temperature in steps of 500 K. The total cooling time is 470 ps with 235×10^3 time steps and a nominal cooling rate of 1×10^{13} K/s. At each temperature, a 20 000 time step relaxation has been allowed. During the first set of 6000 time steps, the velocity is scaled every time step. During the second set of 6000 time steps, velocity scaling every 40 time steps has been performed, and finally, during the last 8000 time steps, no velocity scaling was applied. Data collection has been performed every 50 time steps during the last 15 000 of 35 000 time steps using the microcanonical ensemble NVE.

2.2. Structural Analysis. A glass is a disordered system and its structure can be described in terms of statistical quantities, such as the average bond lengths, coordination numbers (CN), and various distribution functions. The relevant information is contained in the bond-angle distributions (BAD), bridge type distributions for the X−O−X links (where X is a network former ion), Q_n distributions,[42] (where n is the number of bridging oxygens bound to the network former cations), ring size distribution,[43] void size distribution,[41] and wave number dependence of the neutron structure factor $S(q)$. These quantities are analyzed in this paper, and we think that it is convenient for the reader if we give a brief description of the procedure we used here for the calculation of neutron structure factor and fractional free volume (FFV).

According to the standard definitions,[44,45] the partial structure factors are calculated as the Fourier transform of the corresponding partial pair distribution function $g_{ij}(r)$

$$A_{ij}(q) = 1 + 4\pi\rho_0 \int_0^R r^2[g_{ij}(r) - 1] \frac{\sin(qr)}{qr} \frac{\sin(\pi r/R)}{\pi r/R} dr \quad (2)$$

where ρ_0 is the average atom number density. The window function $\sin(\pi r/R)/(\pi r/R)$ has been included to reduce the termination effects resulting from the finite upper limit in the FT of $g_{ij}(r)$.[46] The cut off length R has been chosen to be equal to half of the simulation box edge.

The normalized total-scattering structure factor $S(q)$ is obtained as the weighted sum of the partial structure factors, the weights being the coherent neutron scattering lengths $\bar{b}_i$

$$S(q) = \sum_{ij} c_i c_j \bar{b}_i \bar{b}_j A_{ij}(q) / (\sum_i c_i \bar{b}_i)^2 \quad (3)$$

where $c_i = N_i/N$ is the relative concentration of the i-th species. The following values for the coherent neutron scattering lengths (in Å) have been chosen: $\bar{b}_O = 0.5803 \times 10^{-4}$, $\bar{b}_{Si} = 0.41491 \times 10^{-4}$, $\bar{b}_{Li} = -0.19 \times 10^{-4}$, $\bar{b}_{Na} = 0.363 \times 10^{-4}$, and $\bar{b}_K = 0.367 \times 10^{-4}$.[47]

The free volume (FV) of different glasses have been analyzed in terms of the Delaunay description of the void space into a disordered system.[41] A set of four atoms contiguous to each other forms a tetrahedron called a Delaunay tetrahedron (DT). The whole set of the tetrahedra constructed in this way constitute the Delaunay tessellation, because they fill the space without gaps and without overlaps. Free volume is calculated as the summation of all the void spaces inside the DTs that cover the entire box of the simulation.[41] Therefore, the fractional free volume (FFV) is here defined as the fraction of empty space with respect to the total volume of the box. The analysis of the empty space inside the structure requires that atoms are considered as spheres and that a dimension is assigned to them. We have decided to use as atomic radii the Pauling ionic radii that are 0.60, 0.95, 1.33, 0.41, and 1.40 Å for lithium, sodium, potassium, silicon, and oxygen, respectively.

2.3. Elastic Properties. The elastic properties (Young's modulus E, shear modulus G, bulk modulus B, and Poisson's ratio ν) of the MD simulated glasses can be obtained via energy minimization.[48]

The stiffness matrix elements for a crystalline system are defined as the second derivative of the energy (U) with respect to the strains (ϵ)[49]

$$C_{ij} = \frac{1}{V}\left(\frac{\partial U}{\partial \epsilon_i \partial \epsilon_j}\right) \quad (4)$$

Once the stiffness matrix **C** is obtained, several related mechanical properties of anisotropic materials can be derived from their matrix elements or from the matrix elements of the compliance matrix **S**

$$\mathbf{S} = \mathbf{C}^{-1} \quad (5)$$

The bulk modulus B in the Reuss notation is given by

$$B^{-1} = S_{11} + S_{22} + S_{33} + 2(S_{31} + S_{21} + S_{32}) \quad (6)$$

whereas the shear modulus is given by

$$G = \frac{15}{4(S_{11} + S_{22} + S_{33} - S_{12} - S_{13} - S_{23}) + 3(S_{44} + S_{55} + S_{66})} \quad (7)$$

Poisson's ratios are calculated from the compliance matrix for six components

$$\nu_{xy} = -\frac{S_{21}}{S_{11}}, \nu_{xz} = -\frac{S_{31}}{S_{11}}, ..., \nu_{zy} = -\frac{S_{32}}{S_{33}} \quad (8)$$

The isotropic Poisson's ratio is then obtained by averaging the six components.

(39) Gale, J. D.; Rohl, A. L. *Mol. Simul.* **2003**, *29*, 291.
(40) Malavasi, G.; Pedone, A.; Menziani, M. C. *Mol. Simul.* **2006**, *32* (12−13), 1045.
(41) Malavasi, G.; Menziani, M. C.; Pedone, A.; Segre, U. *J. Non-Cryst. Solids* **2006**, *352*, 285.
(42) Cormack, A. N.; Cao, Y. *Mol. Eng.* **1996**, *6*, 183.
(43) Yuan, X.; Cormack, A. N. *Comput. Mater. Sci.* **2002**, *24*, 343.
(44) Keen, D. A. *J. Appl. Cryst.* **2001**, *34*, 172.
(45) Faber, T. E.; Ziman, J. M. *Philos. Mag.* **1965**, *11*, 153.

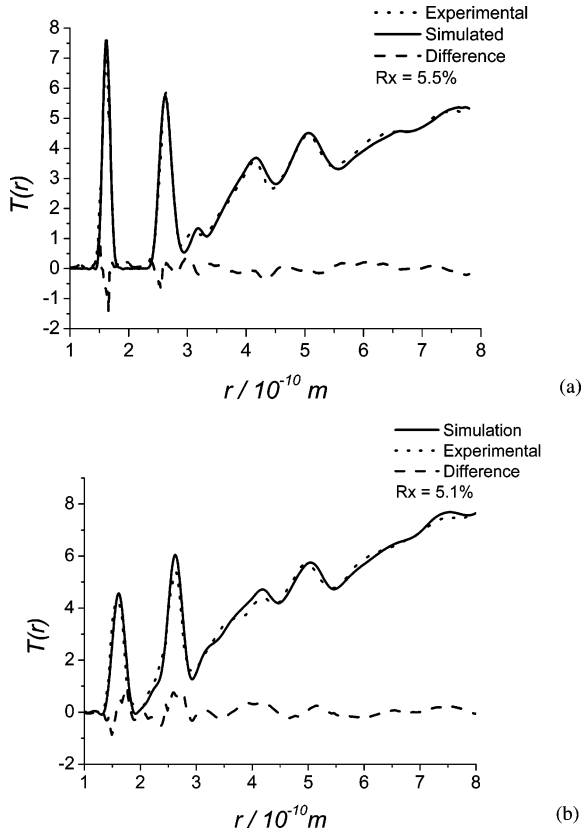

Figure 1. (a) Computed total distribution function of SiO_2 glass, broadened using the experimental $Q_{max} = 45.2$ A^{-1}, compared with the neutron diffraction data digitized from Grimley et al.[55] (b) Computed total distribution function of NS30glass, broadened using the experimental $Q_{max} = 22.88$ A^{-1}, compared with the neutron diffraction data digitized from Wright et al.[21]

The Young's modulus values along three principal directions are given by

$$E_k^{-1} = S_{kk}\,(k = 1,3) \tag{9}$$

For isotropic materials the three principal values must be equal. Moreover, E, G, B and ν must satisfy two relations

$$G = \frac{E}{2(1+\nu)} \text{ and } B = \frac{E}{3(1-2\nu)} \tag{10}$$

therefore, only two independent constants are needed to specify the elastic behavior of an isotropic material.

The elastic properties have been computed for the glasses obtained from the MD simulation runs by means of the GULP code.[39] A Newton−Raphson[50] energy minimization has been performed at constant pressure (1 atm). The coulomb term has been evaluated by means of the Ewald method in which the real cutoff has been determined according to an accuracy of 1×10^{-8}.[51] The minimum image convention has been turned off and the short-range potentials cutoff has been set to 10 Å. The approach of Fletcher and Powell[52] has been used to update the Hessian matrix. It is worth noticing that in static energy-minimization techniques, a different setting of the energy evaluation is necessary than for MD simulations. This is due to the fact that in the minimization technique, only one system configuration is used and the calculation of elastic properties strictly depends on the second derivative of the energy in the local minimum reached. Therefore, a greater accuracy of the calculation is required, which is achieved using the same conditions used for force-field parametrization.[38] To handle the amorphous character of the glass a cubic cell with no symmetry (space group $P1$) has been used which is the MD simulation cell. Several tests have been carried out with simulation boxes of 3000 atoms to check the dependencies on box dimensions.

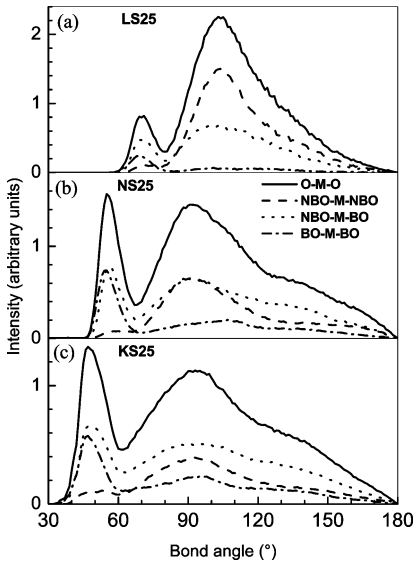

Figure 2. The O−M−O bond angle distributions (continuous line) for three different glasses with similar compositions: (a) LS25, (b) NS25, (c) KS25. The components NBO−M−NBO (dash), NBO−M−BO (dot), BO−M−BO (dash−dot), where M = Li, Na, K are shown for each distribution.

3. Results and Discussion

3.1. Structural Data. An efficient way to summarize and validate the results of the MD simulations of disordered glasses consists of comparing the computed total correlation function $T(r)$ with appropriate diffraction data, the accuracy of the fit being measured by the R_x factor[53]

$$R_x = \left(\frac{\sum_i [T_{exp}(r_i) - T_{sim}(r_i)]^2}{\sum_i T_{exp}^2(r_i)}\right)^{1/2} \tag{11}$$

The $T_{sim}(r)$ has been broadened using the method described by Wright.[54] Panels a and b of Figure 1 show the comparison of the $T(r)$ obtained by the simulated silica and NS30 glasses, respectively, and the corresponding neutron diffraction data.[21,55] The R_x factor, computed over the range $1 \le r \le 8$, is also given in the figures. For the silica glass, a value of $R_x = 5.5\%$ is obtained. Previous simulations[23,24] that made use of Teter, BKS, and Vessal potentials yielded R_x factors of 6.8, 7.2, and 9.3%, respectively; and more recently,[56] an

(46) Lorch, E. A. *J. Phys. C* **1969**, *2*, 229.
(47) Sears, V. F. *Neutron News* **1992**, *3*, 26.
(48) Parker, S. C.; Price, G. D. *Adv. Solid State Chem.* **1989**, *1*, 295.
(49) Ney, J. F. *Physical Properties of Crystals*; Oxford Scientific Publications: Oxford, UK, 1985.
(50) Leach, A. R. *Molecular Modelling: Principle and Applications*; Prentice Hall: London, 2001.
(51) Gale, J. D. *GULP Manual*; Curtin University of Technology: Bentin, Australia, 2005.
(52) Fletcher, R.; Reeves, C. M. *Comput. J.* **1964**, *7*, 149.
(53) Wright, A. C. *J. Non-Cryst. Solids* **1993**, *159*, 264.
(54) Wright, A. C. In *Experimental Techniques of Glass Science*; American Ceramic Society: Westerwille, OH, 1993; p 205.
(55) Grimley, D. I.; Wright, A. C.; Sinclair, R. N. *J. Non-Cryst. Solids* **1990**, *119*, 49.
(56) Tilocca, A.; de Leeuw, N. H.; Cormack, A. N. *Phys. Rev. B* **2006**, *73*, 104209.

Table 3. Bond Lengths and Coordination Numbers (CN) of Alkali Silicate Glasses (the cutoff used to calculate the CNs was 2.0, 2.6, 3.1, and 3.8 for Si−O, Li−O, Na−O ,and K−O, respectively; the results of Du et al.[26] using Teter potentials are reported in brackets)

		M = Li		M = Na		M = K	
	xM_2O (mol %)	bond length (Å)	CN	bond length (Å)	CN	bond length (Å)	CN
Si−O	$x = 0$	1.62	4.0				
M−O	$x = 10$	1.95	3.5	2.31 (2.36)	4.8 (4.4)	2.71(2.76)	7.9 (8.0)
	$x = 15$	1.96 (1.93)	3.6 (3.2)	2.30	4.8	2.69	7.6
	$x = 20$	1.97 (1.95)	3.7 (3.4)	2.31 (2.38)	4.9 (4.7)	2.72 (2.77)	7.6 (7.8)
	$x = 25$	1.97 (1.95)	3.8 (3.5)	2.33	5.2	2.71	7.6
	$x = 30$	1.98 (1.96)	3.9 (3.6)	2.32 (2.39)	5.3 (5.0)	2.69	7.6
M−BO/NBO	$x = 10$	2.09/1.94	1.3/2.2	2.60/2.25	2.8/2.0	2.92/2.66	5.4/2.5
	$x = 15$	2.10/1.95	1.1/2.5	2.60/2.29	2.3/2.5	2.91/2.64	4.5/3.1
	$x = 20$	2.09/1.96	1.0/2.7	2.60/2.30	2.1/2.8	2.91/2.66	4.0/3.6
	$x = 25$	2.08/1.96	1.0/2.8	2.65/2.29	2.0/3.2	2.94/2.66	3.8/3.9
	$x = 30$	2.09/1.97	0.9/3.0	2.58/2.30	1.8/3.5	2.90/2.69	3.4/4.2

R_x factor of 5.2% was obtained by means of shell model. All the results are comparable because they have been obtained using the same experimental q_{max} value of 45.2 Å^{-1}. No defect sites or oddly coordinated oxygen and silicon atoms have been detected in this study. The major contribution to the R_x value can be attributed to the shift in the position of the third peak that results in a calculated Si−Si distance (3.140 Å) that is longer with respect to the experimental one (3.077 Å).

The R_x factor obtained for the NS30 glass is 5.1% (Figure 1b), in good agreement with the values of R_x5.9, 5.1, and 6.8%, respectively, which have been obtained by using Teter, BKS, and Vessal potentials in previous simulations.[23,24] It is worth noting that neither the peak at 4.0 Å nor its lower-right-side shoulder at around 3.7 Å are completely reproduced. A detailed study performed by Yuan and Cormack[57] associates this zone of the $T(r)$ function to the Si−O−Si bond angle and dihedral angle distribution.

Table 3 summarizes the bond lengths and coordination numbers of the simulated glasses obtained in this work, together with the ones previously reported by Du et al.[26] obtained using the Teter potentials. The alkali−oxygen bond lengths have been estimated by the peak position of the alkali−oxygen pair distribution and the CNs have been calculated based on cutoffs obtained from the first minimum of the pair-distribution functions. They are: 2.6 Å for Li−O, 3.1 Å for Na−O, and 3.8 Å for K−O. Bond distances and CNs have been further partitioned into BO and NBO contributions. The Li−O bond length increases from 1.947 to 1.977 Å passing from LS10 to LS30. The coordination number increases from 3.5 to 3.9 and approaches 4 for the disilicate glass. These distances are in excellent agreement with previous calculations by Banhatti and Heuer,[28] who calculated 1.98 Å for the disilicate glass, which compares well with those obtained by Du and Corrales[26] also reported in Table 3. A neutron diffraction isotopic substitution study of the $Li_2Si_2O_5$ glass[17] reported the value 1.97 Å for the average Li−O bond length, with an asymmetric distribution. The coordination number for the narrow component of the distribution is 3.2 ± 0.2, but the presence of additional 0.8 ± 0.5 atoms at longer distances is suggested. Moreover, in crystalline lithium disilicate,[58] the environment of each Li atom is constituted by three NBO atoms at 1.89, 1.97, and 2.03 Å and one BO oxygen atom at 2.10 Å, and a 4-fold coordination for Li with a distorted tetrahedron geometry is assumed. These findings are in agreement with an average coordination number of 3.0 and a distance of 1.968 Å for Li−NBO and an average Li−BO coordination number of 0.9 associated with a distance of 2.090 Å found in this study for LS30.

The Na−O bond lengths range from 2.300 to 2.332 Å, which compare well with EXAFS and neutron diffraction data of 2.30−2.36 Å.[16,59,60] The coordination number of the sodium ions increases from 4.8 to 5.3 for the NS10 and NS30 glasses. Similarly, EXAFS studies by Greaves et al.[60] show a CN of 5 ± 0.5 O for Na ions in sodium disilicate glasses.

The K−O bond length values range between 2.687 and 2.724 Å with a coordination number of 7.9−7.6 in compositions studied. An increase in the K−NBO bond lengths and in the number of NBO around potassium (2.5−4.2) passing from KS10 to KS30 is observed. On the other hand, the K−BO bond length ranges from 2.91 to 2.94, and the number of BO around potassium decreases from 5.4 to 3.4 for KS10 and KS30 glasses, respectively. In the crystalline $K_4Si_8O_{18}$ (0.25 K_2O 0.75 SiO_2, which has the same composition as the KS25 glass), the potassium ions have an irregular oxygen coordination shell; half of them have seven oxygen neighbors with the K−O distances ranging from 2.677 to 3.171 Å (average 2.913 Å), whereas the other potassium ions have six neighboring oxygen atoms with K−O distances ranging from 2.687 to 3.152 Å (average 2.898 Å).[61]

Neutron diffraction experiments carried out on the $(SiO_2)_{0.739}$-$(K_2O)_{0.261}$ glass by Hannon et al.[18] showed a K−O distance of 2.667 Å.

The O−modifier−O bond angle distributions (BADs) and their BO/NBO components are shown in Figure 2. The O−Li−O bond angle distribution for LS25 (Figure 2a) features a minor peak at ∼70° made by NBO−Li−BO and BO−Li−BO, a major peak at 102.5°, mainly constituted by NBO−Li−NBO and NBO−Li−BO, and a broad tail over 120°. Zhao et al.[17] estimated an average O−Li−O bond angle of 103.8°, whereas in the $Li_2Si_2O_5$ crystals,[58] the O−Li−O angle ranges from 83 to 132°, giving an average value of 101.5°. The $Li_2Si_2O_5$ crystal structure shows both edge- and

(57) Yuan, X.; Cormack, A. N. *J. Non-Cryst. Solids* **2003**, *319*, 31.
(58) Smith, R. I.; Howie, R. A.; R., W. A.; Aragon-Pina, A.; Villafuerte-Castrejon, M. E. *Acta Crystallogr., Sect. C* **1990**, *46*, 363−365.
(59) Clare, A. G.; Bachra, B.; Wright, A. C.; Sinclair, R. N. *The Physics of Non-Crystalline Solids*; Taylor and Francis: London, 1992.
(60) Greaves, G. N.; Fontaine, A.; Lagrarde, P.; Raoux, D.; Gurman, S. J. *Nature* **1981**, *293*, 611.
(61) Schweinsberg, H. L. F. *Acta Crystallogr., Sect B* **1974**, *30*, 2206.

Table 4. Q_n Distributions of the Simulated Alkali Silicate Glasses (experimental data in parentheses when available[a])

	n					
	0	1	2	3	4	5
SiO2	0.0	0.0	0.0	0.0	100.0	0.0
LS10	0.0	0.0	1.3 (4)	19.5 (24)	79.2 (73)	0.0
LS15	0.0	0.0	4.8 (8)	25.8 (37)	69.4 (55)	0.0
LS20	0.0	0.0	7.3 (7)	35.1 (50)	57.6 (43)	0.0
LS25	0.0	0.8	10.9 (7)	41.9 (58)	46.3 (35)	0.0
LS30	0.0	2.2	16.5	44.7	36.6	0.0
NS10	0.0	0.0	1.0	20.3	78.7	0.0
NS15	0.0	0.0	4.2	27.1	66.7	0.0
NS20	0.0	0.0	6.1 (2)	37.0 (48)	56.9 (50)	0.0
NS25	0.0	0.3	11.5 (1)	42.7 (61)	45.7 (38)	0.0
NS30	0.0	1.7	16.2 (5)	48.5 (68)	33.5 (27)	0.0
KS10	0.0	0.0	0.9	20.1	78.9	0.1
KS15	0.0	0.2	3.0	28.8	68.0	0.0
KS20	0.0	0.0	6.5	36.9 (49)	56.6 (51)	0.0
KS25	0.0	0.5	11.3	43.0	45.2	0.0
KS30	0.0	2.8	14.8	47.5	34.9	0.0

[a] Experimental data for lithium silicate glasses are from ref 7; those for sodium and potassium silicate glasses are from ref 6.

corner-sharing LiO_4 tetrahedra; the NBO−Li−NBO BAD ranges from 96.6 to 126.3°, while the NBO−Li−BO BAD ranges from 99.5 to 119.9°. No BO−Li−BO angles are present within a cutoff of 2.6 Å.

The O−Na−O BADs, displayed in Figure 2b, show a distinct peak at 60°, a broad peak at around 90°, and a shoulder at 150°, as discussed previously.[23] The main contribution to the first peak are the NBO−Na−BO and BO−Na−BO bond angles, while the NBO−Na−NBO bond angle contributes mainly to the peak at around 90°.

The O−K−O BAD displayed in Figure 2c features a high and sharp peak centered at 47°, a broad peak at 93°, and a shoulder around 135°. The BO−K−BO and NBO−K−BO contributions are mainly responsible for the major peak, whereas the broader peak is due to the NBO−K−BO and NBO−K−NBO contributions. In crystalline $K_4Si_8O_{18}$, the NBO−K−BO BAD peak ranges from 44.2 to 86.5°, the BO−K−BO one ranges from 35.0 to 46.7°, and the NBO−K−NBO one ranges from 85.1 to 131.2°.[61]

The Q_n distributions of the simulated glasses are listed in Table 4. The experimental Q_n distributions are reported in parenthesis for comparison, when available.[6,7] In the simulated glasses, Q_4 decreases and Q_1, Q_2, and Q_3 increase monotonically with increasing Li_2O concentration. No isolated silicon oxygen tetrahedra or 5-fold coordinated silicons were observed. For low alkali concentration, the topology of the silica network is in good agreement with the experimental data.[7] Although the trends in the Q_n variation with composition agree well with the experimental trends, quantitative discrepancies increase with alkali concentration. These discrepancies were also reported by Voigt et al.,[7] who used potentials parameters based on ab initio calculations by Habasaki[62−64] to study medium-range order and Li segregation in lithium silicate glasses.

Most likely, this behavior is due to the lack of polarization terms in the force fields as shown by Tilocca et al.[56] However, the different physical processes between the calculated and experimental cooling, resulting in significantly different glass-transition temperatures, could not be ruled out. In fact, Buckermann et al.[65] pointed out that the discrepancy in the experimental Q_n distribution obtained by different authors might result from the differences in thermal history of the measured glasses.

Analysis of the data listed in Table 4 shows that higher field strength modifiers shift the disproportion reaction $2Q_3 \leftrightarrow Q_2 + Q_4$ to the right. In fact, lithium silicate glasses have fewer Q_3 species and more Q_2 and Q_4 species than sodium silicate glasses with the same alkali molar composition. In their turn, sodium silicate glasses have fewer Q_3 species and more Q_2 and Q_4 species than potassium silicate glasses with the same alkali composition.

We will not further discuss these features here because our results on the Q_n distributions and ring size distributions are in very good agreement with those recently obtained by Du and Corrales using the Teter potential[25,26] and with the work by Voigt et al.[7] for the medium-range order of lithium silicate glasses.

3.2. Elastic Properties. Table 5 lists the computed E, G, B, and ν data values of the alkali silicate glass compositions, together with the experimental data available from the literature.[66]

The data values of the elastic properties are obtained as the average over three simulation runs.

Slightly different values of E in the spatial directions result from the simulations because of clustering of specific ions at the atomic scale. This phenomenon has been outlined previously both from computer simulations studies[7,22,67] and experimental measurements.[68] However, because the E values calculated along the three directions differ by less than 10%, the Young's modulus for each glass is calculated as their average.

It is worth noticing that for lithium silicate systems with small lithium content, NMR experiments show that clustering of Li-rich regions are observed.[7] This clustering is reproduced in the present work even if the dimensions of the box used do not allow a detailed analysis as it was done previously.[67] This clustering seems to increase the differences of the Young's modulus among the three directions, in fact, the greatest difference of 15% was found in the case of LS10 glass. At low alkali content, the degree of isotropy follows the trend K glasses > Na glasses > Li glasses, because the greater differences are 7.5, 13, and 13.0% for the KS15, NS15, and LS15 glasses, respectively. With the addition of modifiers, the degree of isotropy increases in the case of lithium and sodium silicate glasses because the greater differences along the three directions are 8 and 10% in both cases. On the other hand, the degree of isotropy slightly decreases for the KS25 glass, for which the greater difference along the three directions is about 10%. It is worth noticing that when the box dimensions are increased, the material

(62) Habasaki, J. *Mol. Phys.* **1990**, *70*, 513.
(63) Habasaki, J.; Okada, I.; Hiwatari, Y. *Mol. Simul.* **1992**, *9*, 319.
(64) Habasaki, J.; Okada, I.; Hiwatari, Y. *Mol. Simul.* **1993**, *10*, 19.
(65) Buckermann, W. A.; Mulle-Warmuth, W. *Glastech. Ber.* **1992**, *65*, 18.
(66) Manghnani, M. H. In *Handbook of Glass Properties*; Bansal, N. P., Doremus, R. H., Eds.; Academic Press: London, 1986.
(67) Lusvardi, G.; Malavasi, G.; Menabue, L.; Menziani, M. C.; Pedone, A.; Segre, U. *J. Phys. Chem. B* **2005**, *109*, 21586.
(68) Greaves, G. N. *J. Non-Cryst. Solids* **1985**, *71*, 203.

Table 5. Mechanical Properties (E = Young's modulus, G = shear modulus, B = bulk modulus, and ν = Poisson's ratio) for Lithium, Sodium, and Potassium Silicate Glasses Computed with Different Force Fields, FF (refs 38 and 26), with the Priven 2000 Empirical Method[1] and Experimentally Measured Values;[66] (percent errors with respect to experimental data are reported in parentheses; the statistical spreads for the calculated data are ±1.0 GPa, ±0.9 GPa, ±0.6 GPa, and ±0.007 for E, B, G, and ν, respectively)[a]

	experimental data			predicted by FF from ref 38			predicted by FF from ref 26			Priven 2000		
xM$_2$O (mol %)	Li	Na	K	Li	Na	K	Li	Na	K	Li	Na	K
						E (GPa)						
0	72.50	72.50	72.50	72.05 (−0.6)	72.05 (−0.6)	72.05 (−0.6)	81.46 (12)	81.46 (12)	81.46 (12)	68.00 (−6)	68.00 (−6)	68.00 (−6)
10	74.26	65.29		75.46 (2)	64.20 (−2)	56.00	78.49 (6)	71.59 (10)	65.41	70.80 (−5)	59.30 (−9)	59.30
15	76.42	62.90	52.67	73.30 (−4)	61.07 (−3)	53.62 (2)	76.08 (−0.4)	63.51 (1)	63.77 (21)	72.20 (−6)	62.45 (−0.7)	54.95 (4)
20	76.99	61.08	49.04	76.16 (−1)	58.53 (−4)	49.42 (0.8)	79.75 (4)	64.69 (6)	54.67 (12)	73.60 (−4)	60.60 (−0.8)	50.60 (3)
25	78.44	59.77	46.45	78.52 (0.1)	58.13 (−3)	46.59 (0.3)	82.30 (5)	63.22 (6)	49.76 (7)	75.00 (−4)	58.75 (−2)	46.25 (−0.4)
30	78.81	59.33	-	78.74	56.64 (−0.1)	42.56 (−4)	85.68	60.84 (9)	45.30 (2)	76.40	56.90 (−3)	41.90 (−4)
						G (GPa)						
0	31.25	31.25	31.25	30.43 (−3)	30.43 (−3)	30.43 (−3)	33.39 (7)	33.39 (7)	33.39 (7)	29.06 (−7)	29.06 (−7)	29.06 (−7)
10	30.48	27.68	-	31.69 (4)	26.99 (−3)	22.83	32.38 (6)	29.27 (6)	26.55	29.94 (−2)	24.8 (−10)	24.87
15	32.15	26.29	21.62	30.47 (−5)	25.11 (−5)	21.83 (−4)	30.90 (1)	25.55 (−3)	25.43 (18)	30.35 (−6)	26.19 (−0.4)	22.80 (6)
20	31.40	25.18	19.75	30.72 (−2)	23.60 (−6)	20.02 (1)	31.9 (2)	26.02 (3)	21.89 (11)	30.74 (−2)	25.27 (−0.4)	20.74 (5)
25	31.74	24.26	18.43	31.87 (0.4)	23.26 (−4)	18.49 (0.3)	32.81 (3)	24.97 (3)	19.86 (8)	31.11 (−2)	24.36 (−0.4)	18.70 (2)
30	31.73	23.80	-	31.33 (−1)	22.38 (−6)	17.21	34.27 (8)	23.73 (−0.3)	17.76	31.47 (−0.8)	23.46 (−1)	16.69
						B (GPa)						
0	36.10	36.10	36.10	37.94 (5)	37.94 (5)	37.94 (5)	48.38 (34)	48.38 (34)	48.38 (34)	34.34 (−5)	34.34 (−5)	34.34 (−5)
10	43.92	33.95	-	40.55 (−8)	34.67 (2)	29.10	45.33 (3)	42.88 (26)	38.30	37.17 (−15)	34.08 (0.4)	32.11
15	40.89	34.51	31.13	41.03 (0.3)	35.57 (3)	32.90 (6)	46.98 (15)	40.95 (19)	39.72 (28)	38.74 (−5)	33.84 (−2)	31.07 (−0.2)
20	46.81	35.46	31.62	48.66 (4)	37.18 (5)	30.97 (−2)	53.17 (14)	43.58 (23)	36.24 (15)	40.48 (−14)	33.58 (−5)	30.11 (−5)
25	49.43	37.16	32.31	48.84 (−1)	38.52 (4)	32.22 (−0.3)	55.52 (12)	45.33 (22)	34.94 (8)	42.43 (−14)	33.30 (−10)	29.27 (−9)
30	50.92	39.03	-	53.80 (6)	40.13 (3)	31.31	57.14 (12)	46.16 (18)	33.20	44.48 (−13)	33.02 (−15)	28.52
						ν						
0	0.160	0.160	0.160	0.184 (15)	0.184 (15)	0.184 (15)	0.220 (38)	0.220 (38)	0.220 (38)	0.170 (6)	0.170 (6)	0.170 (6)
10	0.218	0.180	-	0.191 (−12)	0.191 (6)	0.226	0.212 (−3)	0.223 (24)	0.232	0.183 (−16)	0.186 (3)	0.192
15	0.158	0.196	0.218	0.203 (29)	0.216 (10)	0.254 (17)	0.231 (46)	0.243 (24)	0.254 (17)	0.189 (20)	0.192 (−2)	0.205 (−6)
20	0.226	0.213	0.242	0.240 (6)	0.240 (0.7)	0.249 (13)	0.250 (11)	0.254 (19)	0.249 (0.7)	0.197 (−13)	0.199 (−7)	0.220 (−9)
25	0.236	0.232	0.260	0.232 (−2)	0.250 (8)	0.263 (0.3)	0.254 (8)	0.266 (15)	0.263 (0.3)	0.205 (−13)	0.206 (−11)	0.237 (−9)
30	0.242	0.247	-	0.252 (6)	0.26 (7)	0.273	0.250 (3)	0.282 (14)	0.275	0.214 (−12)	0.213 (−14)	0.255

[a] Elastic constants for SiO_2 glass ($x = 0$) have been taken from ref 81.

becomes more isotropic and the difference between the three directions decreases. However, no relevant differences have been found for the values of elastic properties of the glasses studied.

Prediction of the elastic properties has been achieved by making use of two different interatomic potential functional forms with partial ionic charges: the one utilized in this paper to obtain the glass structures and described previously[38] and the potential derived by Teter,[26] which employed a Buckingham function and used only oxide structural features in the parametrization process. Comparison with the results obtained by means of several empirical models available in the SciGlass package[35] has also been performed. Table 5 lists the results obtained with the Priven 2000 method,[1] which furnishes the best experimental data predictions. This is an incremental model in which chemical equilibrium factors are derived from the properties of binary and ternary glasses and various property equations are applied, depending on the glass composition and temperature.

Overall good agreement with the experimental data is obtained by both the force fields utilized. However, the Teter's force field[26] gives a systematic positive difference in the prediction of the elastic properties. This result seems to be due to the shape of the energy hypersurface for vitreous

silica, which yields a Si−O bond stiffer than expected from the experimental data. Therefore, in the following, we will restrict the discussion to the results obtained by the force field developed by Pedone et al.[38]

No experimental errors are associated with the data values taken from literature. Being obtained by ultrasonic wave propagation, they are assumed to be quite accurate. The computed Young's modulus values are reproduced with maximal differences with experiment of 4, 4, and 2% for lithium, sodium, and potassium silicate glasses, respectively, whereas shear modulus (G) and bulk modulus (B) show slightly higher differences with maximal values of 6−8%. The larger differences are associated with the Poisson's ratios (υ) for all the glasses studied.

Almost all the elastic properties values predicted with the Priven 2000 empirical method are underestimated. Maximal differences below 9, 10, 15, and 20% have been found for E, G, B, and ν, respectively. Moreover, the bulk modulus in sodium silicate glasses shows an opposite dependence on Na content with respect to the experimental trend and fails to reproduce the plateau at high K concentrations found experimentally.

Despite the great advantage of obtaining a rough estimate of the mechanical properties with a very low computational effort with respect to atomistic simulation techniques, the Priven method does not provide insight into the atomistic structural and dynamical features responsible for the variation of the observed properties. This interpretative aspect is, on the contrary, the main advantage of the atomistic simulations.

In the following, we will focus only on the discussion of E and B. In fact, because G is related to E according to eq 10 and considering that the Poisson's ratios have the same trends and range from 0.16 to 0.26, the approximate relation $G \approx 0.3\ E$ is obtained by substituting the mean value $\nu = 0.22$ in eq 10.

3.2.1. Young's Modulus. It is usually believed that, because of the modifier nature of alkali oxides, their addition to silica glass results in a decreasing of the glass Young's modulus values. In fact, the addition of one network modifier unit M_2O causes one BO bridging between two connected tetrahedra to be replaced by two NBO's, one on each tetrahedron. The presence of NBO determines a break in the linkage within the structure and, therefore, favors the atom's displacements.

On this basis, one should expect E to be directly proportional to the total number of Si−O−Si bridges. However, the results show that this is not the case. In fact, the average percentage of Si−O−Si bridges is not influenced by the chemical nature of the alkali ions.

Vaills et al.[34] claimed that the variation in the values of the elastic moduli of alkali silicate glasses might be the result of two opposite effects: (*a*) the depolymerization of the SiO_2 network by the modifier addition would decrease the cohesion of the SiO_2 chains and consequently would lead to a decrease in the elastic constants; (b) the establishment of new NBO−M−NBO or NBO−M−BO bonds (with M = cation modifier) would promote the cohesion of the glass, leading to an increase in the elastic constants as a function of the concentration of the modifiers.

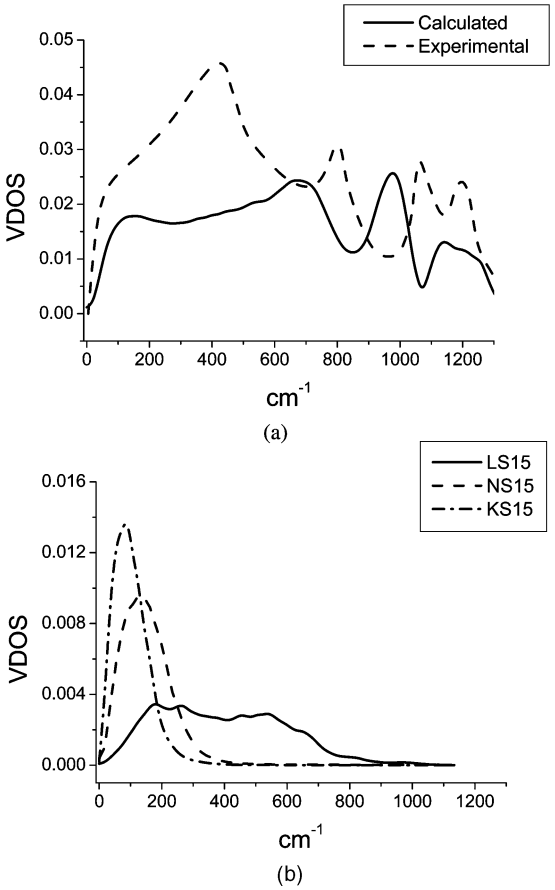

Figure 3. (a) Vibrational density of states (VDOS) for v-SiO_2 and (b) Projection of VDOS for each different modifier of the glasses LS15 (straight line), NS15 (dashed line), and KS15 (dashed−dot line).

It is therefore necessary to understand which of these effects dominates in the systems studied. The strength of the cation modifier−oxygen bond is not easily determined in a glass. Numerical values reported in the literature[69] are computed by assuming a dependence from the coordination number and type of oxygen atoms (BO or NBO) and are derived from crystal phases or glasses with specific composition.

A semiquantitative estimate of the strength of chemical bonds between cations and the surrounding oxygen atoms in the simulated glasses is obtained by the evaluation of force constants via vibrational frequencies. Therefore, the vibrational density of states (VDOS) has been computed in this work by direct diagonalization of the dynamical matrix.[70] Figure 3a shows the comparison of the calculated VDOS for pure SiO_2 with the experimental one.[71] The deficiency of the potentials used results in a shift of the spectrum of the high-frequency region to lower frequencies by ∼100 cm^{-1}. Better results were obtained by Oligschleger[72] and Taraskin et al.[73] even though the pronounced peak in the intermediate frequency region at 415 cm^{-1} was not repro-

(69) Varshneya, A. K. *Fundamentals of Inorganic Glasses*; Academic Press: New York, 1994.
(70) Jin, W.; Vashishta, P.; Kalia, R. K.; Rino, J. P. *Phys. Rev. B* **1993**, *48*, 9359.
(71) Arai, M.; Hannon, A. C.; Taylor, A. D.; Otomo, T.; Wright, A. C.; Sinclair, R. N.; Price, D. L. *Trans. Am. Crystallogr. Assoc.* **1991**, *27*, 113.
(72) Oligschleger, C. *Phys. Rev. B* **1999**, *60*, 3182.
(73) Taraskin, S. N.; Elliott, S. R. *Phys. Rev. B* **1997**, *56*, 8605.

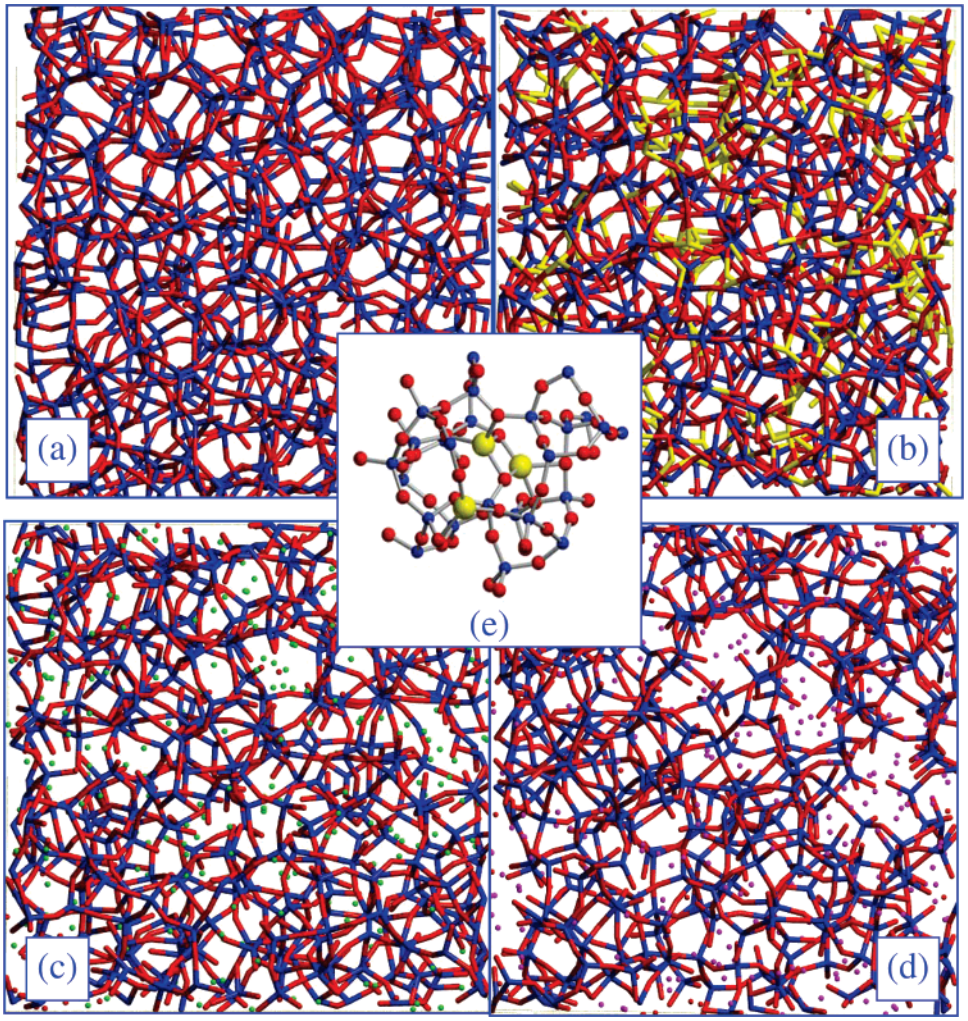

Figure 4. Structural changes in the glass network encountered by the addition of Li (light yellow), Na (light green), and K (light magenta) ions, silicon and oxygen are represented as blue and red sticks, respectively. (a) SiO_2 glass network; (b) LS25 glass network (Li is 4-fold coordinated and seems to act as a network former increasing the polymerization and packing of the structure. Because of its small size and high field strength Li shows a high degree of ion clustering and forms small rings); (c) NS25 glass network (the Na ion is 5-fold coordinated and acts as a modifier disrupting the silica network); (d) KS25 glass network (the K ion is 7−8-fold coordinated, its big size causes the formation of large rings and wide percolation channels are found); (e) picture of the two- and three-membered rings made of 4-fold coordinated Li (light yellow) with silicon (light blue) and with itself.

duced. These discrepancies are not surprising, because the potentials were derived by empirical fitting on structure and mechanical properties of binary oxides and vibrational frequencies were not taken into account.[74] The effect of modifier addition to the projection of VDOS of silicon is not accurately determinable, because it is obscured by the broadening of the bands due to numerical artefacts. However, this effect is weak, and it is reasonable to assume that the strength of the Si−O bond is independent of the type of modifier added. More interesting results are encountered in the projection of VDOS for Li, Na, and K ions, as shown in Figure 3b. The projection of VDOS for Na and K has a log-normal shape, that of K being narrower and shifted to lower frequencies. The K−O frequencies range from 30 to 170 cm^{-1} with a maximum peak at 97 cm^{-1}; Na−O frequencies range from 50 to 250 cm^{-1} with a maximum at 130 cm^{-1}. Li VDOS is spread out over a larger frequency interval that ranges from 100 to 700 cm^{-1}, with two peaks at around 240 and 500 cm^{-1}.

These results can be compared with far-infrared spectra that exhibit a band, called cation mode, characteristic of the interaction between alkali atoms and the NBO atoms in the glass network. The frequency of this band is weakly dependent on the nature of the network forming ion (Si, V, B, P, and Ge) but it is strongly dependent on the nature of the modifier cations.[75] Therefore, the ratio of the force constants of the M−O bonds (with M = Li, Na, K) can be estimated from the ratio of the values of the frequencies of the corresponding bands. The experimental values are: $\bar{\nu}_{Li-O}$ = 347 cm^{-1}, $\bar{\nu}_{Na-O}$ = 180 cm^{-1}, and $\bar{\nu}_{K-O}$ = 113 cm^{-1}.[76] The simulation provides a weaker Na−O bond, which explains the negative differences associated with the prediction of the Young's modulus for sodium silicate glasses. However, both the simulation and experimental data show that the force constant of the cation mode frequencies increases in the order K < Na < Li, in agreement with the ranking of the elastic constants at a fixed alkali concentration.

(74) Pedone, A.; Corno, M.; Civalleri, B.; Malavasi, G.; Menziani, M. C.; Segre, U.; Ugliengo, P. *J. Mater. Chem.* **2007**, *17*, 2061.
(75) Exarhos, G.; Risen, W. M., Jr. *Solid State Commun.* **1972**, *11*, 755.
(76) Hauret, G.; Vaills, Y.; Parot-Rajaona, T.; Gervais, F.; Mas, D.; Luspin, Y. *J. Non-Cryst. Solids* **1995**, *191*, 85.

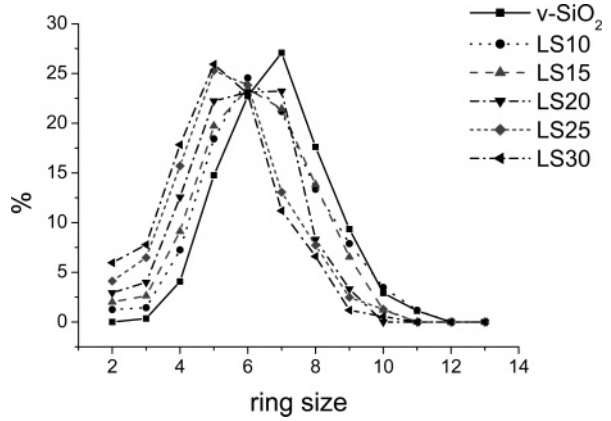

Figure 5. Ring size distribution for lithium silicate glasses calculated by considering Li as pseudo-network former. When Li_2O is added. the maximum shifts to smaller rings, leading to a greater overall cross-linking of the network.

Table 6. Position q_1 and Full Width at Half-Maximum of the First Sharp Diffraction Peak for the Simulated Glasses; Repeat Distance and Correlation Length are Also Reported.

formulation	q_1 (Å^{-1})	fwhm (Å^{-1})	$2\pi/q_1$ (Å)	2π/fwhm (Å)
SiO2	1.575	0.827	3.989	7.598
LS10	1.675	0.752	3.751	8.355
LS15	1.689	0.764	3.720	8.224
LS20	1.727	0.718	3.638	8.751
LS25	1.734	0.717	3.624	8.763
LS30	1.737	0.710	3.617	8.850
NS10	1.673	0.873	3.756	7.197
NS15	1.723	0.898	3.647	6.997
NS20	1.736	0.909	3.619	6.912
NS25	1.754	0.926	3.582	6.785
NS30	1.782	0.939	3.526	6.691
KS10	1.638	0.935	3.835	6.720
KS15	1.746	0.952	3.599	6.600
KS20	1.764	1.002	3.562	6.271
KS25	1.764	1.039	3.562	6.047
KS30	1.780	1.142	3.529	5.500

A visual inspection of the MD-derived glass structures presented in Figure 4 shows that Li addition to silica glass, Figure 4b, leads to an increase in cross-linking and cohesion of the network. In this context, lithium seems to act as a pseudo-network former with 4-fold coordination and high force constant. On this basis, we can obtain an accurate evaluation of the network polymerization by the ring size distribution for lithium silicate glasses reported in Figure 5; in this analysis, Li has been marked as network former. A significant shift of the maximum in the ring size curve to smaller rings as a function of Li concentration is observed. Therefore, the experimentally determined increasing of the elastic constant values with respect to the silica glass is nicely explained as a direct consequence of Li induced network polymerization.

Because of their higher coordination numbers, longer distances and lower force constants Na and K act as purely modifier cations. Their effect on network depolymerization dictates the Young's modulus macroscopic behavior, with E decreasing more sharply for K, which forms larger rings, as shown in Figure 4d.

A further structural property that seems to correlate with the trends observed in the Young's modulus is the correlation length of the first sharp diffraction peak (FSDP).[77,78]

The position of the FSDP (q_1) is related to the atomic arrangement with characteristic repeat distance $d = 2\pi/q_1$

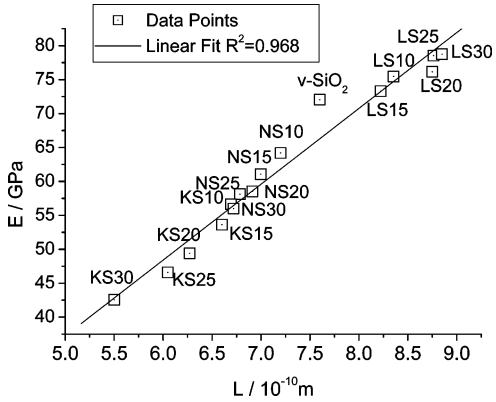

Figure 6. Linear correlation between the experimental Young's modulus and the correlation length of FSDP of the simulated glasses.

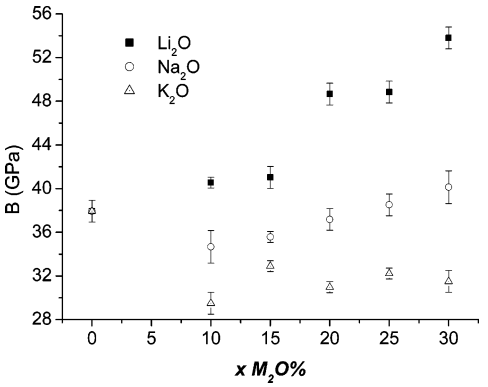

Figure 7. Calculated Bulk modulus (B) as a function of alkali ion concentration. The error bars denote the range of data values.

and the full width half-maximum (fwhm) is interpreted as resulting from the regions of atomic density fluctuation with the correlation length $L = 2\pi$ /fwhm.

The main features of the FSDP for the glasses studied in this paper are listed in Table 6. The decrease in the characteristic repeat distances and the characteristic correlation lengths as a function of Na and K content indicates that the intermediate-range order decreases with alkali oxide concentration. The opposite behavior showed by lithium silicate glasses could be due to the ability of its high field strength to order the surrounding network and modifier regions.

The quantitative rationalization of the Young's modulus modulation by dopant addition reported in Figure 6 promotes the correlation length as an eligible descriptor both for quantitative predictions and interpretation of the structure dependence of the Young's modulus for the alkali silicate glasses. It is worth noting that the structural analysis carried out on the simulate glasses fully support the intuitive hypothesis advanced by Vaills et al.[34]

3.2.2. Bulk Modulus and Fractional Free Volume. According to the model by Vaills et al.[34] mentioned above, the same trends are to be expected for E and B as a function of the alkali ions concentration. According to the discussion in the previous section, B should increase for lithium silicate glasses and decrease for sodium and potassium silicate

(77) Gottlicher, J.; Pentinghaus, H. J. *Ber. Bunsen−Ges. Phys. Chem. 9* **1996**, *9*, 1563.
(78) Zotov, N.; Keppler, H.; Hannon, A. C.; Soper, A. K. *J. Non-Cryst. Solids* **1996**, *202*, 153.

glasses. However, both the simulation results reported in Figure 7 and the experimental data show a different behavior. Indeed, in lithium silicate glasses, *B* increases from 36 GPa for v-SiO_2 to 51 GPa for LS30 glass, whereas in sodium silicate glasses, it initially decreases for low Na_2O concentrations, according to the expectation, but it overcomes the value of pure silica at 25% Na_2O concentration, with an overall increase of about 3 GPa. In the case of potassium silicate glasses, *B* greatly decreases for the first addition of K_2O, and then a slight increase is observed, though the value of pure silica is never reached.

The structural analysis of the MD simulated glasses suggests that in addition to the depolymerization of the SiO_2 network and the establishment of new NBO−M bonds, a third effect must be taken into account to explain this complex behavior. This additional effect is related to the decrease of the fractional free volume (FFV) in an amorphous solid as a consequence of alkali addition. In fact, the greater the FFV, the greater the compressibility, because a large free volume corresponds to a low packing density and therefore to an easier compressibility of the material. Therefore, an inverse proportionality between the FFV and *B* values is expected. The FFV values have been computed according to the algorithm we have recently developed.[41] It was found that FFV varies quite linearly ($r^2 = 0.999$ for each series of data) with the dopant content *x*. The angular coefficients *m* of the linear regression have the following values: $m_{Li} = -0.1559$, $m_{Na} = -0.1313$, $m_K = -0.1174$. These results show that the FFV decreases with an increase in the alkali concentration (and therefore *B* increases). Moreover, this effect is more marked for Li than for Na than for K, in qualitative agreement with the experimental finding for the bulk modulus.

Recently, Hannemann et al.[79] showed that in the case of the amorphous high-temperature ceramic *a*-$Si_3B_3N_7$, a strong correlation between the density, the energy and the bulk modulus is observed. Models with the same chemical composition, generated by different synthesis routes exhibit different densities and bulk modulus. Ito et al.[80] reported similar findings in the case of soda-lime glasses. They studied the effects of cooling rate on the structure and properties and showed that glasses cooled at higher rate are less polymerized and exhibit smaller rings and smaller Si−O−Si bond angles, therefore, smaller density and smaller Young's modulus.

The role of thermal history in determining the final density and physical properties of the glasses is extremely important from a computational point of view and should be extensively addressed. However, in this paper, we were concerned with the optimization of methods to calculate reliable elastic properties from computer simulations, and therefore, models generated via constant volume simulations to fix the experimental density during quenching were utilized for subsequent constant pressure minimization and computation of the second derivative of the energy with respect to positional and cell strains. After the minimization, the densities result with a typical error of +2−3% with respect to the experimental ones. The trends in the FFV variation with composition calculated on the samples before and after constant pressure minimization were shown to be very similar, because the minimization does not affect the Si−O network topologies (ring size distributions and Q_n distributions) but leads to an increase in the density through the decrease in the Si−O−Si angles.

4. Conclusions

The combined molecular dynamics simulations and energy-minimization study carried out in this work has allowed the correct quantitative evaluation of the elastic properties of several series of alkali silicate glasses. The excellent agreement between the simulation results and the experimental data testifies to a prediction performance superior to those of the empirical methods commonly used in the glass scientific community. However, the main advantage of atomistic simulations over empirical methods rests in their ability to deepen the interpretative levels obtained from the experiments by providing atomic level pictures of the glass structures and detailed insight into composition−atomic structure relationships. In particular, the balance among three concurrent factors with differing consequences on the glass network seems to be responsible for the compositional dependence of the mechanical properties observed experimentally in the series of glasses studied. These factors are (1) depolymerization of the silica network that leads to a decrease in the elastic constants; (2) increasing the cohesion of the glass by the establishment of alkali−NBO bonds that lead to an increase in the elastic constants as a function of the chemical nature and concentration of the modifiers; and (3) decreasing the free volume with consequent increasing in the glass pack density, leading to a minor compressibility and therefore to a greater bulk modulus.

Starting from this framework, a quantitative description of the relationship between structure and elastic properties will be derived in the enlarged set of samples.

Acknowledgment. This work was supported by Ministero dell'Istruzione, Università e Ricerca, (MIUR, Grant 2003032158_005).

CM062619R

(79) Hannemann, A.; Schon, J. C.; Jansen, M.; Putz, H.; Lengauer, T. *Phys. Rev. B* **2004**, 70, 144201.
(80) Ito, S.; Taniguchi, T. *J. Non-Cryst. Solids* **2004**, *349*, 173−179.
(81) Hwa, L. G.; Hsieh, K. J.; Liu, L. C. *Mater. Chem. Phys.* **2003**, *78*, 105.